

Thermodynamic Benefits of Opposed-Piston Two-Stroke Engines

2011-01-2216

Published
09/13/2011

Randy E. Herold, Michael H. Wahl, Gerhard Regner and James U. Lemke
Achates Power, Inc.

David E. Foster
Univ. of Wisconsin - Madison

Copyright © 2011 SAE International

doi:[10.4271/2011-01-2216](https://doi.org/10.4271/2011-01-2216)

ABSTRACT

A detailed thermodynamic analysis was performed to demonstrate the fundamental efficiency advantage of an opposed-piston two-stroke engine over a standard four-stroke engine. Three engine configurations were considered: a baseline six-cylinder four-stroke engine, a hypothetical three-cylinder opposed-piston four-stroke engine, and a three-cylinder opposed-piston two-stroke engine. The bore and stroke per piston were held constant for all engine configurations to minimize any potential differences in friction. The closed-cycle performance of the engine configurations were compared using a custom analysis tool that allowed the sources of thermal efficiency differences to be identified and quantified. The simulation results showed that combining the opposed-piston architecture with the two-stroke cycle increased the indicated thermal efficiency through a combination of three effects: reduced heat transfer because the opposed-piston architecture creates a more favorable combustion chamber area/volume ratio, increased ratio of specific heats because of leaner operating conditions made possible by the two-stroke cycle, and decreased combustion duration achievable at the fixed maximum pressure rise rate because of the lower energy release density of the two-stroke engine. When averaged over a representative engine cycle, the opposed-piston two-stroke engine had 10.4% lower indicated-specific fuel consumption than the four-stroke engine.

In a second analysis, the closed-cycle simulation was extended to a engine system model to estimate the pumping work required to achieve the operating conditions needed to reach a specified NO_x emissions rate. Because the opposed-

piston two-stroke engine has inherently lower peak in-cylinder temperatures than the four-stroke engine, lower intake pressure was required to meet the NO_x emissions constraint and as a result lower pumping work was needed. At the simulated condition considered, the opposed-piston two-stroke engine had approximately 9.0% lower brake-specific fuel consumption than the four-stroke engine.

INTRODUCTION

Opposed-piston two-stroke engines were conceived in the 1800's in Europe and subsequently developed in multiple countries for a wide variety of applications including aircraft, ships, tanks, trucks, and locomotives and maintained their presence throughout most of the twentieth century [1,2,3,4,5]. An excellent summary of the history of opposed-piston engines can be found in reference [1]. Produced initially for their manufacturability and high power density, opposed-piston two-stroke engines have demonstrated superior fuel efficiency compared to their four-stroke counterparts. This paper examines the underlying reasons for the superior fuel efficiency by investigating and quantifying the thermodynamic benefits of the opposed-piston two-stroke engine relative to a reference four-stroke engine.

Comparisons of this nature are challenging because the outcome depends strongly on the underlying assumptions that need to be both defensible and unbiased. Therefore, the comparison put forth in this paper is constructed in the follow manner. First, the influence of friction is eliminated by constructing the engine architectures to have an equal number of pistons, equal bore diameters, and equal strokes per piston. A reference six-cylinder four-stroke engine is "rearranged" into a hypothetical three-cylinder opposed-piston four-stroke

engine and then to a three-cylinder opposed-piston two-stroke engine by removing the cylinder head and forming new cylinders while keeping bore and stroke per piston unchanged. By preserving the base geometry, any differences in power cylinder and bearing friction between the engine architectures are minimized, and, considering that the valve-train friction of the four-stroke engine is traded against the gear-train friction of the opposed-piston engine, friction differences are eliminated to a first order from this comparison.

Second, the comparison between the engine configurations is initially focused on the closed portion of the engine cycle using a custom zero-dimensional (0D) thermodynamic engine analysis tool that quantifies the losses due to in-cylinder heat rejection, temperature-dependent gas properties, and combustion phasing relative to an ideal engine cycle consisting of isentropic compression/expansion and isochoric combustion. This analysis, provided in Part I of the paper, provides a fundamental thermodynamic comparison of the engine configurations by ignoring any potential differences in the in-cylinder scavenging and in the pumping work required to achieve the prescribed boundary conditions. All operational parameters, such as compression ratio, manifold conditions, engine speed, power requirements, and maximum pressure rise rate, are applied equally to all engine architectures. Simulation results are presented for a number of operating conditions over a representative speed/load engine operating map.

Third, an additional comparison is provided in Part II of the paper that extends the analysis to include pumping losses by using an engine system model to consider an aircharge system comprised of turbo machinery, charge air coolers, and an EGR loop. This additional analysis was included to account for the engine pumping losses and to assess the true impact of the thermodynamic advantage of opposed-piston two-stroke engines on the overall engine efficiency. The scavenging performance of each engine was again assumed to be perfect, although an additional constraint of equivalent engine out NOx was assigned in order to determine the intake pressure and EGR rate for the engine system simulations.

BACKGROUND - IDEAL ENGINE EFFICIENCY

When comparing thermodynamic efficiencies of various engine configurations, it is useful to understand the maximum possible closed-cycle efficiency ("ideal engine efficiency") that an internal combustion engine can achieve, for two reasons. First, the assumptions underlying the ideal engine analysis help identify the practical considerations that lead an engine not to achieve the maximum possible closed-cycle efficiency. Second, the ideal engine provides an efficiency limit to which the calculated closed-cycle efficiencies can be compared. Both of these factors will be discussed below and

will be incorporated into the comparison between the engine configurations.

The internal combustion engine cycle that achieves the ideal efficiency is conceptualized using the pressure-volume state diagram provided in [Figure 1](#), where the pressure and volume values are plotted on logarithmic axes. The process between state (1) and state (2) represents isentropic (*i.e.*, adiabatic and reversible) compression from the maximum cylinder volume (V_1) to the minimum cylinder volume (V_2), where the compression ratio is defined as $r_c = V_1/V_2$. The process from state (2) to state (3) represents adiabatic and isochoric (constant volume) combustion, and the process from state (3) to state (4) represents isentropic expansion. The working fluid is assumed to be calorically perfect, with γ being the constant ratio of specific heats.

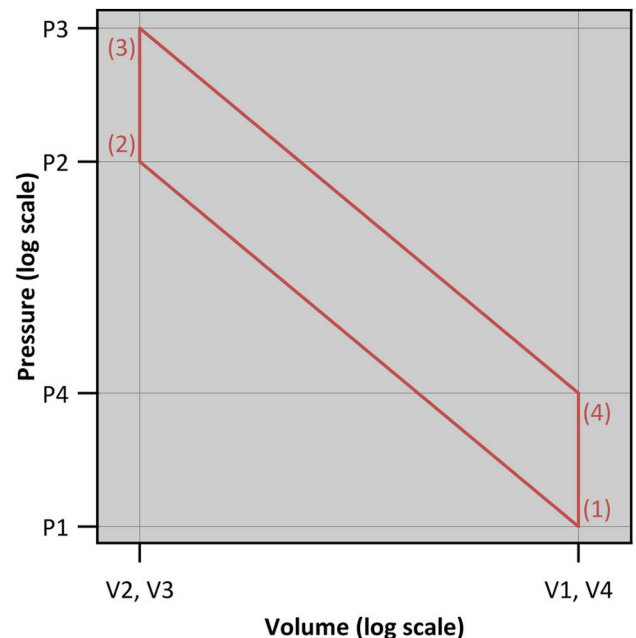


Figure 1. Pressure-volume state diagram of an ideal engine achieving the maximum possible closed-cycle thermodynamic efficiency.

Using the assumptions listed above, an energy balance can be evaluated from state (1) to state (4), and from this energy balance the equation for the ideal engine efficiency, η_{ideal} , shown in [Equation 1](#), can be derived [6]. Only two variables, the compression ratio (r_c) and ratio of specific heats (γ), remain after simplification of the equation. Increasing the compression ratio increases the operating volume over which compression and expansion occur, and increasing the ratio of specific heats increases the pressure rise during combustion and increases the work extraction per unit of volume expansion during the expansion stroke. Both effects result in an increase in the net system work for a given energy release and thereby increase the engine efficiency.

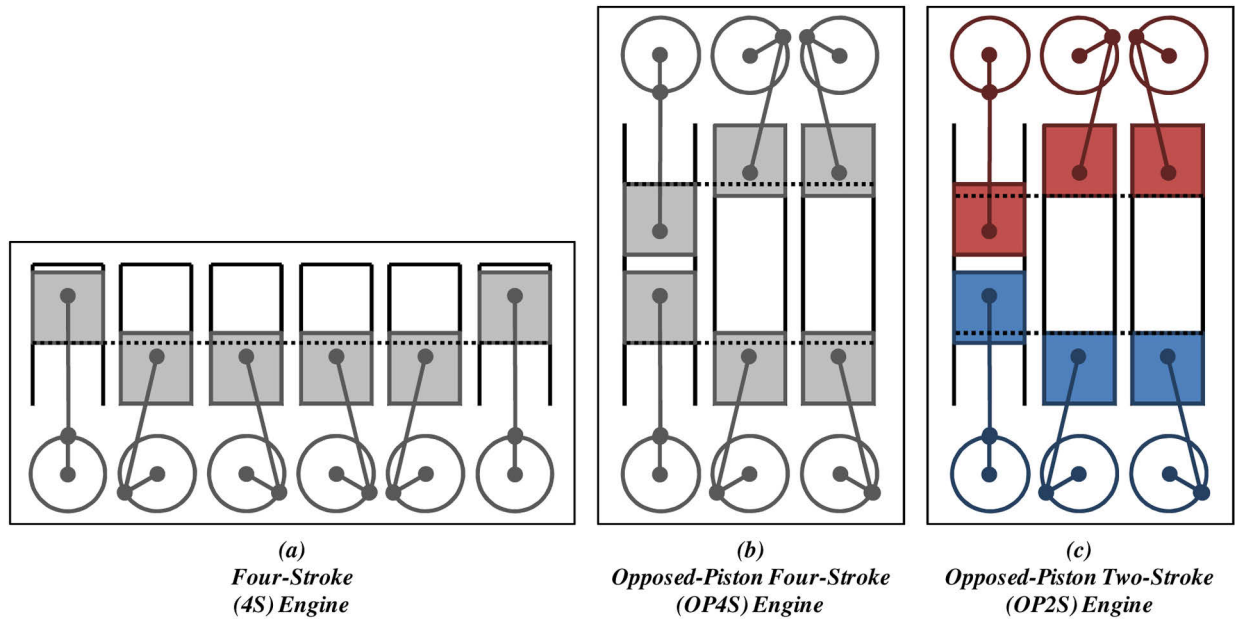


Figure 2. Schematics of the (a) four-stroke, (b) opposed-piston four-stroke, and (c) opposed-piston two-stroke engines considered in this study.

$$\eta_{ideal} = 1 - \frac{1}{r_c^{\gamma-1}} \quad (1)$$

It should be noted that the process from state (4) to (1) represents the exhaust process in which available energy is rejected from the cylinder. This available energy can be converted to mechanical or electrical work via an additional hardware component external to the combustion chamber, although at additional system cost and complexity. Modern compression-ignition engines almost universally use one such device (a turbocharger, where a turbine converts a portion of the available energy to work that drives a mechanically connected compressor), although more sophisticated configurations, such as turbocompounding, bottoming cycles and thermoelectric generators, have been mentioned as possible methods to further utilize this available energy [7,8].

Practical engine considerations and temperature-dependent fluid properties lead actual closed-cycle efficiencies to deviate from the ideal engine efficiency. First, the assumption of isochoric combustion does not apply because of the finite duration combustion that occurs for all realistic combustion regimes. Even for kinetically controlled combustion, which can achieve substantially shorter combustion durations than with Diesel or spark-ignited combustion, the combustion duration will ultimately be limited by mechanical constraints of the engine. Short combustion durations lead to high pressure rise rates that result in audible engine noise and high mechanical stresses to engine components, both of which need to be avoided for engines in commercial vehicles. Second, the assumption of a calorically perfect fluid does not

apply because the specific heats decrease with increasing gas temperature. Additionally, the species conversion that occurs during combustion causes the mixture γ to decrease, a further deviation from the constant γ assumption. Finally, the assumption of an adiabatic combustion chamber does not apply because of the large temperature gradient that occurs in the working fluid near the combustion chamber surfaces, which results in energy being lost to heat transfer rather than being converted to crank work.

ENGINE CONFIGURATIONS

Three engine configurations were considered in this study: a six-cylinder four-stroke (4S) engine with a standard crank-slider architecture and fixed cylinder heads, a hypothetical three-cylinder opposed-piston four-stroke (OP4S) engine, and a three-cylinder opposed-piston two-stroke (OP2S) engine. To keep the friction work associated with each engine as similar as possible, the cylinder bore diameter and stroke per piston were held constant for each engine configuration. Only the engine architecture and valve/port timings were varied, the latter of which was changed to account for the scavenging period of the OP2S engine. Additionally, the power output and engine speed were held constant for all subsequent thermodynamic comparisons. A schematic of each engine configuration is provided in [Figure 2](#).

The standard 4S engine was arbitrarily specified as a six cylinder engine with total trapped volume of 6.0 L (1.0 L per cylinder). The engine power was specified to be 300 hp at a rated engine speed of 2400 rpm. This engine size and peak power output is representative of a number of commercially available engines designed for medium-duty applications

[9,10,11], although no specific engine was used as a basis for the geometry of the baseline four-stroke engine in this study.

A two-dimensional geometric representation of the 1.0 L per cylinder 4S engine was created in an analysis spreadsheet assuming a standard crank-slider relationship with zero lateral piston-pin offset. Along with the total trapped volume of 1.0 L, the 4S architecture was defined by assuming a stroke-to-bore ratio of 1.1 and a trapped compression ratio of 15:1; these values are consistent with published values for both modern and historical turbocharged compression-ignition engines [6,9]. Additionally, the following geometry assumptions were made: the piston crowns and cylinder heads were flat and parallel (*i.e.*, pancake-shaped combustion chamber), the piston pin was 60 mm from the piston crown, the intake valve closed 180° before top dead center, the exhaust valve opened at 180° after top dead center, and the connecting rod length was 3.5 times the crank radius. To finalize the engine geometry, the crank radius and distance between the crankshaft and cylinder head were iteratively solved to achieve the prescribed trapped cylinder volume and compression ratio under the assumptions listed above.

Although there are many viable methods to articulate the pistons in an opposed-piston engine [1], a mechanism that contains two crankshafts - each of which articulates one of the pistons with a crank-slider motion - was selected for the present study. This mechanism, which has been used in successful OP2S engines in the past [4,5,12], was selected because of its simplicity and because the motion of an individual piston is exactly the same for each engine configuration. With this arrangement, the opposed-piston architecture is analogous to placing two cylinders of the standard 4S engine cylinder-head-to-cylinder-head and then eliminating the cylinder head surfaces, thereby combining the two four-stroke cylinders into one opposed-piston cylinder. Schematics of the opposed-piston architecture are shown in Figures 2b and 2c for the OP4S and OP2S engines, respectively.

With the crank radius, connecting rod length, and piston-pin-to-crown distance set to the same values as the 4S engine, the spacing between the engine crankshafts of the OP4S was specified to achieve the desired 15:1 trapped compression ratio assuming that the intake valves close at 180° before top dead center and assuming zero phase offset between the two crankshafts. The former was assumed to match the intake valve closing crank angle of the standard 4S engine, although the feasibility of creating a realistic valve mechanism for this hypothetical OP4S engine is not addressed. It was assumed that the exhaust valves open at 180° after top dead center for the expansion ratio to be equal to the compression ratio.

For the OP2S engine configuration, the crankshaft spacing was specified to achieve the desired 15:1 trapped compression ratio, again assuming the crank radius,

connecting rod length, and piston pin-to-crown distance remained unchanged. For this engine, however, the crank angle at which the intake port closed was delayed to 120° before top dead center, a modification included to account for the scavenging period required for two-stroke engine operation. The specified intake port closing (IPC) crank angle is consistent with IPC values for OP2S engines found in the literature [12]. The crank angle at which the exhaust port opens (EPO) was advanced to 120° after top dead center so the expansion ratio matched the compression ratio, the same assumption used in the 4S and OP4S engines. The phase offset between the two crankshafts was set to 13.5 degrees, a geometric feature required to phase the exhaust and intake port profiles of the two-stroke engine cycle. The specified value is consistent with phase offset values found in the literature [12].

A summary of the geometric characteristics for the three engine configurations is provided in Table 1. As discussed previously, the bore, stroke-per-piston, trapped compression ratio, connecting rod length, and piston pin-to-crown distance values were held constant for all three engine configurations. Because of the delayed intake port-closing crank angle, the total trapped volume per cylinder decreased from 2.0 L in the OP4S to 1.6 L in the OP2S engine. Additionally, the engine stroke, measured as the maximum piston separation minus the minimum piston separation for opposed-piston architectures, decreased by 1.5 mm for the OP2S configuration compared to the OP4S configuration because of the phase offset between the crankshafts.

Table 1. Nominal geometric characteristics for the engines considered in this study.

Engine	4S	OP4S	OP2S
Cylinder Count	6	3	3
Bore (mm)	102.6	102.6	102.6
Stroke per Piston (mm)	112.9	112.9	112.9
Engine Stroke (mm)	112.9	225.7	224.2
Trapped Volume (L/cylinder)	1.0	2.0	1.6
Total Trapped Volume (L)	6.0	6.0	4.8
Trapped Compression Ratio	15:1	15:1	15:1
Clearance Volume (mm ³)	6.7e4	1.3e5	1.1e5
Crank Radius (mm)	56.4	56.4	56.4
Connecting Rod Length (mm)	197.5	197.5	197.5
Pin-to-Crown Distance (mm)	60	60	60
Head-to-Crank Distance (mm)	322.0	---	---
Crank-to-Crank Distance (mm)	---	644.0	639.8
Crankshaft Phase Offset (deg)	---	0	13.5
Intake Closing (deg aTDC)	-180	-180	-120
Exhaust Opening (deg aTDC)	180	180	120

PART I - CLOSED-CYCLE ANALYSIS

QUANTIFICATION OF NON-IDEAL EFFECTS

A custom zero-dimensional (0D) thermodynamic engine analysis tool was created in spreadsheet software and was used to predict the closed-cycle thermodynamic performance of the four-stroke (4S), opposed-piston four-stroke (OP4S), and opposed-piston two-stroke (OP2S) engine configurations. A custom tool was created for this analysis because it could more easily incorporate the engine geometries defined above and because it could provide a more complete and detailed analysis of the closed-cycle thermodynamics than is offered by commercially available software. A complete description of the mathematical equations used by the 0D analysis tool to predict the cylinder pressure during the engine closed cycle is provided in the [Appendix](#).

To quantify the magnitude of the non-ideal effects that lead actual closed-cycle efficiencies to deviate from the ideal engine efficiency, the 0D simulation concurrently calculated the closed-cycle performance for four cases: (1) isochoric (constant volume) combustion, calorically perfect fluid, and adiabatic combustion chamber; (2) finite duration combustion, calorically perfect fluid, and adiabatic combustion chamber; (3) finite duration combustion, variable specific heats, and adiabatic combustion chamber; and (4) finite duration combustion, variable specific heats, and non-adiabatic combustion chamber. The difference in thermal efficiency between case (2) and case (1) represents the loss in thermal efficiency associated with finite duration combustion and is given the symbol $\Delta\eta_{comb}$. The difference in thermal efficiency between case (3) and case (2) represents the loss in thermal efficiency associated with variable specific heats of the fluid (*i.e.*, variable γ) and is given the symbol $\Delta\eta_{\gamma}$. The difference in thermal efficiency between case (4) and case (3) represents the loss in thermal efficiency associated with heat transfer and is given the symbol $\Delta\eta_{ht}$.

[Figure 3](#) illustrates the predicted pressure, energy release rate, ratio of specific heats (γ), and heat transfer rate for the four simulation assumptions at a given operating condition in the four-stroke engine. Note that four curves are present in each plot, but some curves lie identically on top of each other and therefore are not visible. Case 1, which operates with ideal-engine assumptions, shows an extremely rapid pressure rise at top dead center to a peak cylinder pressure of 322 bar (the pressure ordinate was truncated to highlight the lower three curves), which is a result of the energy release occurring over one crank angle increment of the simulation. Case 2 has a more realistic peak cylinder pressure of 163 bar that results from energy release having finite duration ($\Delta\theta_{10-90} = 30$ degrees). The peak cylinder pressure for Case 3 is further reduced to 138 bar, a result of the fluid properties having

temperature- and species-varying γ values. The pressure achieved after compression is lower because of the variable γ , as is the pressure rise during combustion. Case 4 has the lowest peak cylinder pressure, 135 bar, of the four cases because some of the released energy is lost to heat through the combustion chamber surfaces instead of being stored in the in-cylinder charge and raising the cylinder pressure.

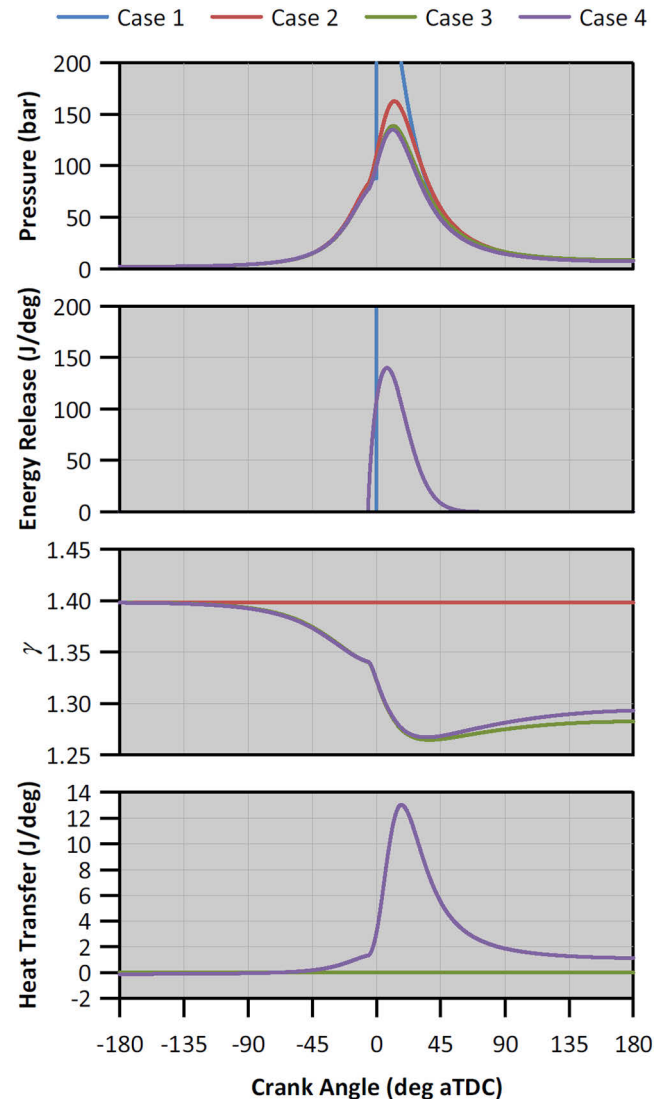


Figure 3. Pressure, energy release rate, γ , and heat transfer results from the 0D simulation of the 4S engine for the four cases discussed in the text.

The thermal efficiency values for the closed-cycle simulations presented in [Figure 3](#) are provided in [Table 2a](#), and the corresponding $\Delta\eta_{comb}$, $\Delta\eta_{\gamma}$, and $\Delta\eta_{ht}$ values are provided in [Table 2b](#). The efficiency values are provided with units of “%_{fuel}” so as to differentiate them as units of thermal efficiency. Note that the thermal efficiency calculated using the 0D analysis tool for Case 1 ($\eta = 66.0$ %_{fuel}) identically equals the efficiency calculated using [Equation 1](#) for a 15:1

trapped compression ratio and a γ value of 1.398, validating the results obtained with the 0D analysis tool. The results in [Table 2b](#) show that for the engine operating condition in [Figure 3](#), the losses in thermal efficiency due to finite duration combustion, variable γ , and heat transfer were 4.6 %_{fuel}, 7.4 %_{fuel}, and 6.5 %_{fuel}, respectively. The sum of the efficiency loss values equals the difference in thermal efficiency between Case 1 and Case 4, as defined.

Table 2. Calculated (a) thermal efficiency and (b) loss in efficiency values from the 0D simulation of the 4S engine for the four simulation cases provided in [Figure 3](#).

(a)		(b)	
Case 1	$\eta = 66.0$ % _{fuel}	$\Delta \eta_{comb} = -4.6$ % _{fuel}	
Case 2	$\eta = 61.3$ % _{fuel}	$\Delta \eta_{\gamma} = -7.4$ % _{fuel}	
Case 3	$\eta = 53.9$ % _{fuel}	$\Delta \eta_{ht} = -6.5$ % _{fuel}	
Case 4	$\eta = 47.5$ % _{fuel}		

RESULTS

Peak Power

The input parameters for simulated peak power engine condition are provided in [Table 3](#). The simulation was run with an assumed engine speed of 2400 rpm, and the fueling rate was adjusted for each engine configuration to achieve an indicated power of 300 hp. The trapped charge conditions were set to a pressure of 2 bar and a temperature of 350 K assuming the pre-combustion charge was only air. The piston and cylinder head metal temperatures were set to 550 K, and the liner metal temperature was set to 450 K. The start of combustion crank angle (θ_{SOC} , see [Equation A15](#)) was varied so that the crank angle of 10% energy release (CA10) occurred at top dead center for all simulations, and the combustion duration ($\Delta\theta_{10-90}$) was varied to achieve a maximum pressure rise rate (MPRR) of 5.1 bar/deg, which was the MPRR value that resulted from a 30 degree combustion duration in the four-stroke engine simulation.

Table 3. Input parameters for the 0D simulation tool at the simulated peak power condition. The parameters were held constant for all engine architectures.

Condition	Peak Power
Engine Speed (rpm)	2400
Indicated Power (hp)	300
Trapped Pressure (bar)	2
Trapped Temp. (K)	350
Trapped Composition	Air
Piston/Head Metal Temp. (K)	550
Liner Metal Temp. (K)	450
CA 10 (deg aTDC)	0
MPRR (bar/deg)	5.1

The simulated pressure results plotted versus cylinder volume on logarithmic coordinates for the four-stroke (4S), opposed-piston four-stroke (OP4S), and opposed-piston two-stroke (OP2S) engines are provided in [Figure 4](#) and indicate the operating volumes over which the simulations were performed. The relevant cycle-averaged results are provided in [Table 4](#) and show that the OP4S engine has a 2.6 %_{fuel} higher indicated thermal efficiency than the 4S engine at the peak power condition while maintaining essentially the same peak cylinder pressure and peak cylinder temperature. The OP2S engine has a 5.5 %_{fuel} higher indicated thermal efficiency compared to the 4S engine with the added benefit of 10% lower peak cylinder pressure and 18% lower peak cylinder temperature.

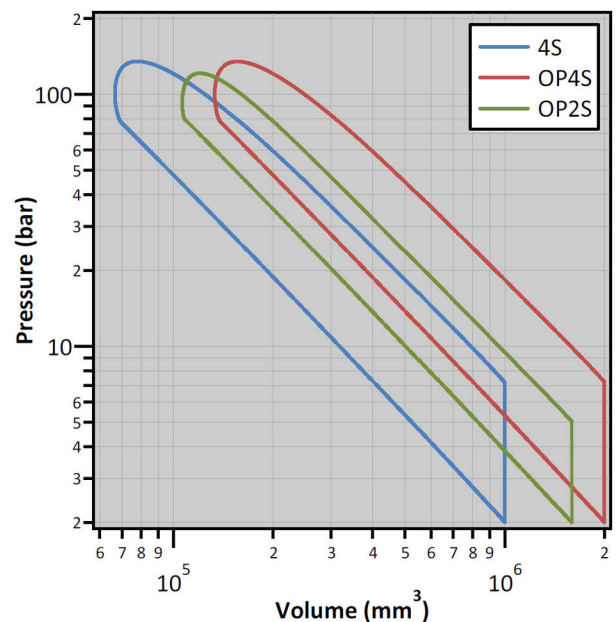


Figure 4. Simulated pressure results for the 4S, OP4S, and OP2S engine configurations at the operating conditions defined in [Table 3](#).

Table 4. Steady-state results for the 4S, OP4S, and OP2S engine configurations at the operating conditions defined in [Table 3](#).

Engine	4S	OP4S	OP2S
Fuel Mass (mg/cycle/cyl)	91.4	173.1	81.8
$\Delta \theta_{10-90}$ (deg)	30.0	28.9	17.8
η (% _{fuel})	47.5	50.1	53.0
Peak Pressure (bar)	135	135	121
Peak Temp. (K)	2095	2099	1724
Trapped λ	1.50	1.59	2.68
$\Delta \eta_{comb}$ (% _{fuel})	-4.6	-4.4	-2.4
$\Delta \eta_{\gamma}$ (% _{fuel})	-7.4	-7.2	-5.4
$\Delta \eta_{ht}$ (% _{fuel})	-6.5	-4.3	-5.2

When comparing the 4S and OP4S engine configurations, it is apparent that the primary factor leading to the increased thermal efficiency for the OP4S engine is reduced heat transfer. The efficiency loss due to heat transfer goes from $-6.5\%_{\text{fuel}}$ to $-4.3\%_{\text{fuel}}$, a decrease of $2.2\%_{\text{fuel}}$, and the reason for the decreased heat transfer can be seen in [Figure 5](#), which shows the area/volume ratio for the three engine configurations. The area/volume ratio is significantly smaller for the OP4S engine than the 4S, a result of combining two of the 4S cylinders into one OP4S cylinder and thereby removing the cylinder head. By reducing heat transfer losses, the fueling rate required to achieve the power target is reduced, as shown in [Table 4](#), which in turn results in leaner in-cylinder conditions and a smaller change in γ during combustion as shown in [Figure 6](#). This change decreases the loss in efficiency due to variable γ by $0.2\%_{\text{fuel}}$. Additionally, the reduced fueling rate allows for the combustion duration to be reduced slightly while maintaining the desired maximum pressure rise rate (see [Table 4](#)). The energy release fraction curves are shown in [Figure 7](#). The $\Delta\theta_{10-90}$ value can be 1.1 degrees shorter for the OP4S engine compared to the 4S engine at the same MPRR, a change that decreases the loss in efficiency due to finite duration combustion by $0.2\%_{\text{fuel}}$.

For the OP2S engine, the doubled firing frequency of the two-stroke cycle adds to the efficiency gains realized by the opposed-piston architecture. Because the two-stroke cycle allows the engine to fire on every engine revolution instead on every other revolution, the fueling rate per engine cycle is reduced roughly by half. For the closed-cycle simulation, in which the trapped conditions were held constant, the result is a much leaner in-cylinder charge. As [Table 4](#) shows, the trapped fuel-air equivalence ratio (λ) value increases from 1.50 and 1.59 for the 4S and OP4S engines, respectively, to 2.68 for the OP2S engine. The result of the leaner in-cylinder charge is a $2.0\%_{\text{fuel}}$ decrease in the efficiency loss due to variable γ compared to the 4S engine and a $1.8\%_{\text{fuel}}$ decrease compared to the OP4S engine. The smaller decrease in γ during combustion is visible in [Figure 6](#).

An added positive effect of the reduced fuel per cycle associated with the two-stroke cycle is that the energy release per unit combustion-chamber volume (energy release density) is reduced, which allows for a much shorter energy release duration without exceeding the maximum pressure rise rate constraint. The energy release density for the 4S engine was 0.059 J/mm^3 , and the $\Delta\theta_{10-90}$ required to meet the 5.1 bar/deg MPRR limit was 30 degrees. For the OP2S engine, the energy release density was 0.033 J/mm^3 , which allowed $\Delta\theta_{10-90}$ to be reduced to 17.8 degrees while still meeting the MPRR limit. By reducing the combustion duration, the energy release more optimally phased near top dead center (see [Figure 7](#)), and the loss in efficiency due to finite-duration

combustion decreases $2.2\%_{\text{fuel}}$ compared to the 4S engine and $2.0\%_{\text{fuel}}$ compared to the OP4S engine.

The inherent geometric advantage of the opposed-piston engine with respect to heat transfer is maintained in the OP2S engine. The area/volume ratio is not as small for the OP2S engine compared to the OP4S (see [Figure 5](#)) since the delayed intake port closing results in a smaller trapped volume, but the OP2S area/volume ratio is still significantly smaller than the standard 4S engine. This effect, combined with shorter combustion duration that causes higher temperatures for a larger portion of the exhaust stroke, results in the loss in efficiency due to heat transfer to increase $1.1\%_{\text{fuel}}$ for the OP2S engine compared to the OP4S engine. Compared to the 4S engine, however, the loss in efficiency due to heat transfer is still $1.3\%_{\text{fuel}}$ lower. There is a trade-off between the loss in efficiency due to heat transfer and the loss in efficiency due to finite duration combustion, so as the combustion duration is lengthened, the loss in efficiency due to finite-duration combustion increases, but the loss in efficiency due to heat transfer decreases.

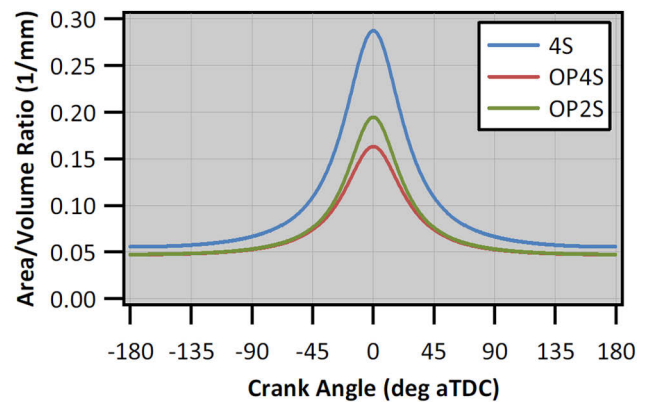


Figure 5. Area/volume ratio comparison for the three engine configurations.

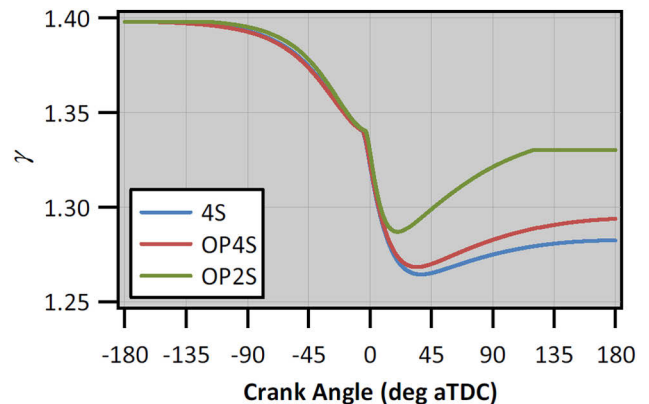


Figure 6. Simulated ratio of specific heats (γ) at the operating conditions defined in [Table 3](#).

Table 5. Operating conditions for the simulated speed/load engine map.

Condition	A25	A100	B50	C25	C100
Weighting (%)	13.9	22.2	27.8	13.9	22.2
Engine Speed (rpm)	1600	1600	2000	2400	2400
Indicated Power (hp)	56.2	224.7	132.7	75	300
Indicated Torque (N-m)	250	1000	472.5	222.5	890.1
Trapped Pressure (bar)	1.25	2	1.5	1.25	2
Trapped Temp. (K)	350	350	350	350	350
Trapped Composition	Air	Air	Air	Air	Air
Piston/Head Metal Temp. (K)	480	530	520	500	550
Liner Metal Temp. (K)	380	430	420	400	450
CA 10 (deg aTDC)	0	0	0	0	0
MPPRR (bar/deg)	2.5	6.0	3.4	2.1	5.1

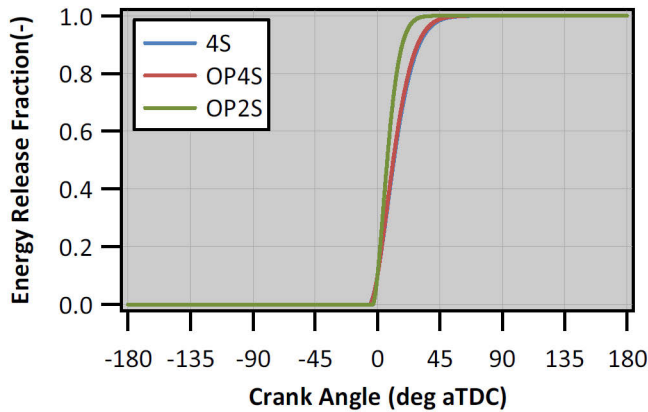


Figure 7. Energy release fraction for the three engine configurations that achieved the desired maximum pressure rise rate.

Weighted-Average

A range of operating conditions was simulated for a speed/load operating map representative of a medium-duty engine. The operating conditions considered for this set of simulations are provided in Table 5. The peak power (C100) condition assumed an indicated engine power of 300 hp (*i.e.*, the same condition considered above), the peak torque (A100) condition assumed an indicated engine torque of 1000 N-m, and a linear torque rise was assumed between these two conditions. The other operating conditions considered were C25, B50, and A25. The weighting factors used to calculate the weighted-average results were taken from the 13-mode SET cycle [13] and normalized to reflect the reduced number of simulation points.

All input parameters were held constant at a given operating condition for the two engine configurations considered (4S and OP2S), but certain parameters were varied over the operating map as shown in Table 5. The trapped pressure was raised with higher engine loads to reflect the necessity of

increased air mass when increasing the fuel mass. The metal temperatures were varied with speed and load: higher metal temperatures with higher load conditions and higher engine speeds. The specified MPPRR limit varied for each operating condition, the value of which was determined by the specified $\Delta\theta_{10-90}$ values in the 4S simulation.

The 0D simulation results for the 4S and OP2S engines at the operating conditions described above are provided in Table 6. For all of the conditions considered in the operating map, the OP2S engine maintains its thermal efficiency benefit over the 4S engine in addition to having lower peak cylinder pressures and peak cylinder temperatures. The increased thermal efficiency again results from a combination of reduced losses in efficiency due to finite duration combustion, variable γ , and heat transfer. The indicated-specific fuel consumption (ISFC) advantage of the OP2S versus the 4S engine ranges from 6.3% at the C25 condition to 12.3% at the A100 condition, and the weighted average ISFC advantage is 10.4%.

PART II - ENGINE SYSTEM ANALYSIS

ENGINE SYSTEM MODEL

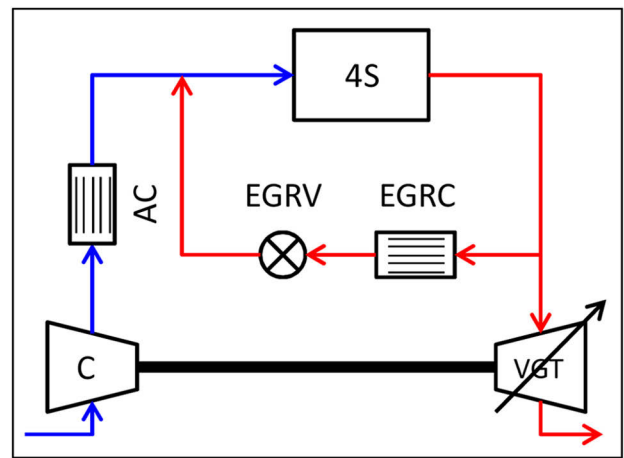
To evaluate the pumping work differences between the engine configurations, engine system models were created for the four-stroke (4S) and opposed-piston two-stroke (OP2S) engines in the commercially available GT-POWER systems modeling software. Schematics of the engine system layout for each engine are provided in Figure 8. In the engine system models, the cylinders were modeled using “mean-value” cylinders, which allowed user-specified input values of indicated thermal efficiency, exhaust energy fraction, and volumetric efficiency instead of relying on the software package to predict the closed-cycle performance. This modeling strategy facilitated the use of the 0D close-cycle simulation to define the indicated performance of the engine.

Table 6. Steady-state simulation results for the 4S and OP2S engines at the five operating conditions considered. The cycle-average ISFC is 10.4% lower for the OP2S engine compared to the 4S engine.

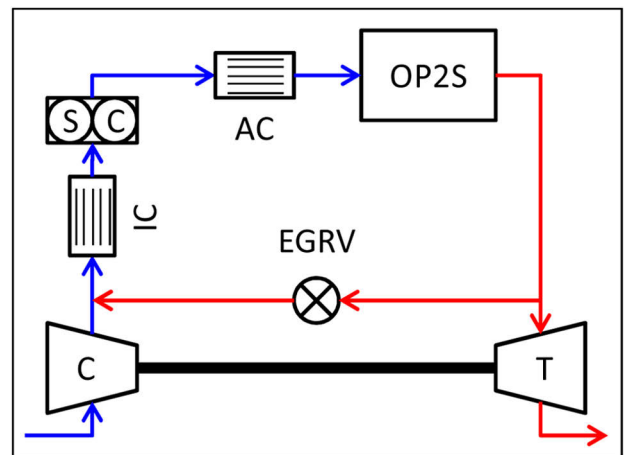
Condition	A25		A100		B50		C25		C100	
Engine	4S	OP2S								
Fuel Mass (mg/cycle/cyl)	25.4	23.4	109.1	95.8	47.7	43.3	21.5	20.2	91.4	81.8
$\Delta\theta_{10-90}$ (deg)	17.9	11.0	29.8	17.7	24.0	14.5	17.9	11.1	30.0	17.8
η (%fuel)	48.0	52.1	44.7	50.9	48.3	53.1	50.3	53.7	47.5	53.0
Peak Pressure (bar)	70	65	146	129	92	84	66	62	135	121
Peak Temp. (K)	1527	1337	2255	1840	1797	1522	1448	1283	2095	1724
Trapped λ	3.37	5.86	1.25	2.29	2.15	3.80	3.97	6.79	1.50	2.68
$\Delta\eta_{comb}$ (%fuel)	-2.0	-1.1	-4.6	-2.3	-3.2	-1.7	-2.0	-1.2	-4.6	-2.4
$\Delta\eta_{\gamma}$ (%fuel)	-4.7	-3.4	-8.2	-5.9	-6.1	-4.4	-4.2	-3.1	-7.4	-5.4
$\Delta\eta_{ht}$ (%fuel)	-11.3	-9.4	-8.5	-6.8	-8.3	-6.8	-9.4	-8.0	-6.5	-5.2
ISFC (g/kW-hr)	174.4	160.9	187.6	164.6	173.3	157.7	166.5	156.0	176.5	158.0
ISFC Benefit vs. 4S (%)	---	7.7	---	12.3	---	9.0	---	6.3	---	10.5

In the engine system models, the compressors (C), supercharger (SC), and turbines (T & VGT) were modeled as “simple” components in which the isentropic efficiency is a constant input parameter instead of being determined by a supplier's performance map. The turbomachinery components were modeled in this manner so as not to bias the results by improper component selection. For the 4S engine, it was assumed that a variable-geometry turbine (VGT) was necessary to create the back pressure required to supply the prescribed EGR rate. Conversely, a fixed-geometry turbine (T) is sufficient for the OP2S engine because the EGR is introduced upstream of the supercharger, which acts as an EGR pump. The compressors, supercharger, and fixed-geometry turbine were given isentropic efficiencies of 0.7. The VGT was given an isentropic efficiency of 0.65, an efficiency decrease typical of such a device.

The charge coolers - intercooler (IC), aftercooler (AC), and EGR cooler (EGRC) - were modeled with zero pressure drop, a fixed effectiveness of 0.9, and a constant coolant temperature of 350 K. Connections between the hardware components were all volume elements so as to eliminate influences, positive or negative, of pressure wave dynamics in the intake and exhaust systems. Precompressor and post-turbine boundary conditions were set as ambient.



(a). Four-Stroke Engine System



(b). Opposed-Piston Two-Stroke Engine System

Figure 8. Schematics of the engine system layouts for the (a) four-stroke and (b) opposed-piston two-stroke engines.

To make the pumping work comparison reflect actual engine operation, an additional constraint of constant engine-out NOx emissions was applied. Instead of specifying a certain NOx level that must be achieved, surrogate constraints in peak in-cylinder temperature of 1600 K and a trapped oxygen mole fraction of 16.3% were used. Both temperature and oxygen content are important parameters in NOx formation, as described in the rate equations of the Zeldovich mechanism [6]. To achieve the peak temperature and oxygen content constraints, the intake pressure varied between the engine configurations, and the trapped composition was assumed to be a mixture of air and EGR. The engine speed, indicated power, intake temperature, metal temperatures, CA10, and MPRR values were the same as provided in Table 3.

The 0D simulation tool was used to determine the intake pressure, EGR rate, indicated thermal efficiency, exhaust energy fraction, air mass flow rate, and fuel mass flow rate required to achieve the constant parameters defined above. The results from the 0D simulation tool were used to determine the exhaust pressure for each engine configuration, the value of which was required to calculate the pumping work needed to achieve the desired operating condition.

In the 4S engine system model, the turbine effective diameter and EGR valve angle were varied to achieve the desired intake pressure and EGR rate when assuming that the engine aspirated a volume of charge equal to the entire cylinder volume each engine cycle. The thermodynamic work associated with the open-cycle pumping loop was calculated for the 4S engine by assuming that the exhaust and intake pressures were applied to the piston face during the entire exhaust and intake strokes, respectively.

For the OP2S engine, the air and EGR mass flow rates were determined by assuming that a volume of charge equivalent to the entire OP2S cylinder volume was delivered to the engine and perfect-displacement scavenging was achieved. The mass flow rate of charge delivered to the engine was then used to calculate the exhaust pressure by assuming that the cylinder acted as an orifice governed by compressible flow theory and through which the mass flow rate was a function of the pressure ratio across the cylinder [12,14]. The effective flow area of the orifice was assumed to be 4% of the bore area, a value that is consistent with both historical uniflow-scavenged engines and in-house test results [14,15]. In the OP2S engine system model, the turbine effective diameter was adjusted to achieve the calculated exhaust pressure for the specified air mass flow rate. This exercise was equivalent to sizing the appropriate fixed geometry turbine to the OP2S engine at the peak engine power condition. Finally, the input power to the simulated supercharger and the EGR valve position were varied in the model to achieve the desired flow rate requirements. Because there is no pumping loop in the two-stroke cycle, the pumping work required to achieve the

desired conditions is equal to the work required to drive the supercharger.

RESULTS

The simulated pressure results, plotted versus volume on logarithmic coordinates, for the 4S and OP2S engine system simulations are provided in Figure 9. The pumping loop was added to the 4S plot for completeness and to show how the intake and exhaust pressures were used to calculate the 4S pumping work. The relevant cycle-averaged results are provided in Table 7 and show that the OP2S requires lower pumping work to achieve the peak power operating conditions while meeting the NOx-equivalent constraints (*i.e.*, peak temperature and oxygen mass fraction). In addition, the thermal efficiency advantage of the OP2S engine over the 4S engine is maintained while still having lower peak cylinder pressure.

The reduced pumping work is a result of the inherently lower peak cylinder temperature for a given intake pressure in the OP2S engine and is also a result of the aircharge system employed. Using a supercharger with a fixed-geometry turbine appears to be a more efficient method for pumping EGR than using a variable-geometry turbine. If the work required to overcome friction is assumed to be 4 %_{fuel}, the brake thermal efficiency for this condition would be 41.5 %_{fuel} for the 4S engine and 45.6 %_{fuel} for the OP2S engine. The 4.1 %_{fuel} (= 45.6 %_{fuel} - 41.5 %_{fuel}) brake thermal efficiency advantage for the OP2S engine is equivalent to a 9.0% reduction in the brake-specific fuel consumption.

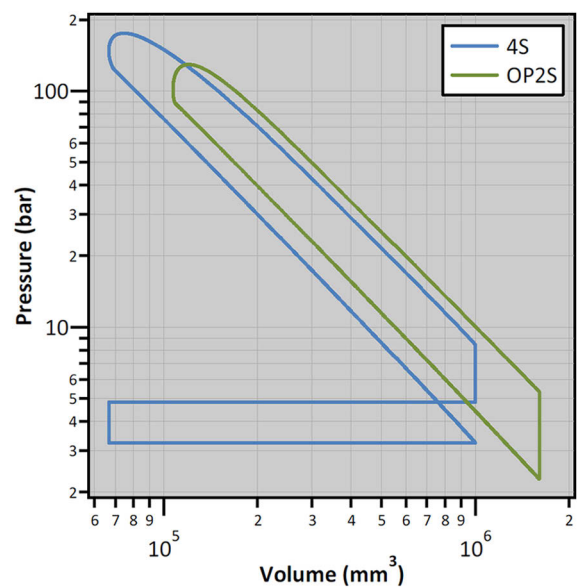


Figure 9. Simulated pressure results for the 4S and OP2S engine configurations at the operating conditions necessary to meet peak power with the additional NOx emission constraints.

Table 7. Steady-state results for the 4S and OP2S engine configurations at the operating conditions necessary to meet peak power with the additional NOx emission constraints.

Engine	4S	OP2S
Intake Pressure (bar)	3.24	2.28
Exhaust Pressure (bar)	4.80	2.02
Air Mass Flow Rate (kg/hr)	969.9	1043.9
EGR Mass Flow Rate (kg/hr)	529.2	684.5
EGR Rate (%)	35.3	39.6
Trapped x_{O_2} (%)	16.3	16.3
Fuel Mass (mg/cycle/cyl)	87.8	82.0
$\Delta\theta_{10-90}$ (deg)	28.8	17.2
η (% _{fuel})	49.4	52.9
Peak Pressure (bar)	175	129
Peak Temp. (K)	1600	1600
Trapped λ	1.98	2.39
$\Delta\eta_{comb}$ (% _{fuel})	-4.4	-2.3
$\Delta\eta_{\gamma}$ (% _{fuel})	-5.9	-5.3
$\Delta\eta_{fr}$ (% _{fuel})	-5.6	-4.8
Pumping Work (% _{fuel})	3.9	3.3

CONCLUSION

A detailed thermodynamic analysis was performed to demonstrate the fundamental efficiency advantage of an opposed-piston two-stroke engine over a standard four-stroke engine of comparable power output and geometric size. A custom, zero-dimensional (0D) thermodynamic engine analysis tool was used to study the closed-cycle performance of a standard four-stroke (4S) engine, a hypothetical opposed-piston four-stroke (OP4S) engine, and an opposed-piston two-stroke (OP2S) engine. Each engine was assumed to have equivalent mechanical friction. The OP4S engine was found to have increased indicated thermal efficiency compared to the 4S engine primarily because of the more favorable area/volume ratio created by the opposed-piston architecture. In addition to the geometric advantage of the opposed-piston architecture, the OP2S engine benefitted from two factors that were enabled by the doubled firing frequency of the two-stroke engine cycle: leaner operating conditions that maintained a higher ratio of specific heats (γ) during combustion, and reduced energy release densities that allowed for shorter combustion durations without exceeding maximum rate of pressure rise constraints. When evaluated over a representative engine speed/load operating map, the OP2S engine achieved 10.4% lower weighted-average indicated-specific fuel consumption than the 4S engine at the same boundary conditions while operating with lower peak pressure and temperature.

Since leaner operating conditions typically require additional pumping work, a GT-POWER engine system model was used in conjunction with the 0D engine analysis tool to investigate the pumping work necessary to produce the intake pressure, exhaust pressure, and EGR rate required in meeting a NOx-equivalent constraint (peak temperature equal to 1600 K and trapped oxygen mole fraction equal to 16.3%). This engine system analysis showed that because the OP2S engine had inherently lower peak cylinder temperatures, the intake pressure could be reduced while still meeting the NOx-equivalent constraint relative to the 4S engine. As a result, the pumping work required to produce the operating conditions was lower for the OP2S engine (3.3 %_{fuel}) than for the 4S engine (3.9 %_{fuel}). Based on an assumed friction work of 4 %_{fuel}, the brake-specific fuel consumption of the OP2S was 9.0% lower than the 4S engine at the simulated peak power condition.

REFERENCES

1. Pirault, J.-P. and Flint, M., "Opposed Piston Engines: Evolution, Use, and Future Applications", SAE International, Warrendale, PA, ISBN 978-0-7680-1800-4, 2009, doi: [10.4271/R-378](https://doi.org/10.4271/R-378).
2. Barsanti, E. and Matteucci, F., "Motore a Pistoni Contrapposti", Piedmont Patent 700, July 26, 1858.
3. Barsanti, E. and Matteucci, F., "Improved Apparatus for Obtaining Motive Power from Explosive Compounds", Great Britain Patent 3270, December 31, 1861.
4. Junkers, H., "Cylinder of Internal-Combustion Engines and Other Similar Machines", U.S. Patent 1 231 903, July 3, 1917.
5. Junkers, H., "Engine", U.S. Patent 2 031 318, February 18, 1936.
6. Heywood, J.B., "Internal Combustion Engine Fundamentals", McGraw-Hill, Inc., New York, ISBN 0-07-028637-X, 1988.
7. TIAX, LLC, "Assessment of Fuel Economy Technologies of Medium- and Heavy-Duty Vehicles", Report to the National Academy of Sciences, 2009.
8. Committee to Assess Fuel Economy Technologies for Medium- and Heavy-Duty Vehicles, National Research Council, Transportation Research Board, "Technologies and Approaches to Reducing the Fuel Consumption of Medium- and Heavy-Duty Vehicles", The National Academies Press, Washington, D.C., ISBN 0-309-14983-5, 2010.
9. DeRaad, S., Fulton, B., Gryglak, A., Hallgren, B., et al., "The New Ford 6.7L V-8 Turbocharged Diesel Engine," SAE Technical Paper [2010-01-1101](https://doi.org/10.4271/2010-01-1101), 2010, doi: [10.4271/2010-01-1101](https://doi.org/10.4271/2010-01-1101).
10. Cummins, Inc., "Cummins Every Time - On-Highway - Medium-Duty Truck - EPA 2010 ISB6.7", <http://>

cumminsengines.com/every/applications/medium_duty_trucks/EPA_2010_ISB67_MDT.page, March 2010.

11. Navistar, Inc., "MaxxForce 7 | Commercial Engine | Diesel Engine", http://maxxforce.com/Application/on-highway/Engine/MaxxForce_7, March 2010.

12. Schweitzer, P.H., "Scavenging of Two-Stroke Cycle Diesel Engines", The Macmillan Co., New York, 1949.

13. DieselNet, "Heavy-Duty Supplemental Emissions Test (SET)", <http://www.dieselnet.com/standards/cycles/set.php>, March 2010.

14. Taylor, C.F., "The Internal-Combustion Engine in Theory and Practice - Volume 1: Thermodynamics, Fluid Flow, Performance", pg. 232, The M.I.T. Press, Cambridge, MA, ISBN 978-0262700269, 1985.

15. Regner, G., Herold, R. E., Wahl, M. H., Dion, E., Redon, F., Johnson, D., Callahan, B. J., and McIntyre, S., "The Achates Power Opposed-Piston Two-Stroke Engine: Performance and Emissions Results in a Medium-Duty Application", SAE Technical Paper [2011-01-2221](https://doi.org/10.4271/2011-01-2221), 2011, doi: [10.4271/2011-01-2221](https://doi.org/10.4271/2011-01-2221).

16. McBride, B.J., Zehe, M.J., Gordon, S., "NASA Glenn Coefficients for Calculating Thermodynamic Properties of Individual Species", NASA/TP - 2002-211556, 2002.

ISFC

Indicated-Specific Fuel Consumption

MRR

Maximum Pressure Rise Rate

NO_x

Oxides of Nitrogen

OP2S

Opposed-Piston Two-Stroke

OP4S

Opposed-Piston Four-Stroke

SET

Supplemental Emissions Test

CONTACT INFORMATION

Randy Herold
herold@achatespower.com

DEFINITIONS/ABBREVIATIONS

4S

Four-Stroke

0D

Zero-Dimensional

CA10

Crank Angle of 10% Energy Release

EGR

Exhaust Gas Recirculation

EPO

Exhaust Port Opening

IPC

Intake Port Closing

APPENDIX

ZERO-DIMENSIONAL CLOSED-CYCLE ANALYSIS TOOL

The pressure rise for a given crank angle is determined by [Equation A1](#), which is derived from a closed-system energy balance where combustion is represented as an energy addition to the system and ideal gas behavior is assumed. Mass addition to the system ([Equation A2](#)) from fuel injection is assumed to be constant from the user-specified start of injection crank angle (θ_{SOI}) and over the injection duration ($\Delta\theta_{inj}$). The volume versus crank angle relationship ([Equation A3](#)) and the volume derivative ([Equation A4](#)) are determined using the engine geometries described above. The fluid temperature is determined using the ideal gas equation of state ([Equation A5](#)) and the gas constant (R_i) for the mixture ([Equation A6](#)). The pressure and mass values are integrated over the closed portion of the engine cycle using [Equations A7](#) and [A8](#), respectively. The initial conditions of pressure (p_0), temperature (T_0), and composition ($x_{n,0}$ for all five species considered - N₂, O₂, Ar, CO₂, and H₂O) are user-specified and determine the initial trapped mass (m_0). For the closed-cycle analysis the initial composition was assumed to be air only, although any arbitrary amount of trapped residual mass could be specified.

During the simulated combustion event, the species mole fraction ($x_{n,i}$) is calculated by [Equation A9](#), which dictates that each species changes from its pre-combustion mole fraction ($x_{n,0}$) to post-combustion mole fraction ($x_{n,b}$) following the combustion burn fraction curve ($x_{b,i}$) discussed below. The post-combustion composition was determined using stoichiometry assuming complete combustion of the delivered fuel mass. Minor species resulting from dissociation during combustion were not considered in this simulation. The mixture molecular weight (MW_i) is calculated as the mole-fraction-weighted average of individual species' molecular weights, as shown in [Equation A10](#).

The mixture specific heat capacity ($c_{p,i}$) was calculated as the mass-fraction-weighted average of the specific heat capacity of the five individual species, as shown in [Equation A11](#). The mass fractions of the individual species are calculated using [Equation A12](#), and the specific heat capacities for individual species ($c_{p,n,i}$) were calculated using the empirical curve fits found in [16]. [Equation A13](#) provides the curve fit equation, and [Table A1](#) provides the coefficients for the five species of interest. The ratio of specific heats (γ_i) is calculated using the mixture specific heat capacity, as shown in [Equation A14](#).

The energy release in the 0D closed-cycle simulation was modeled using the Wiebe combustion burn fraction curve ($x_{b,i}$) shown in [Equation A15](#), and the resulting energy release rate is calculated by [Equation A16](#), where m_f is the mass of fuel delivered and LHV_f is the fuel's lower heating value. The Wiebe combustion model was used because it allowed the combustion phasing and duration to be specified using only two parameters: the start of combustion crank angle (θ_{SOC}) and the crank angle duration between 10% and 90% energy release ($\Delta\theta_{10-90}$). The exponent in the Wiebe combustion profile (m_c) was given a value of 0.7, which created an asymmetric combustion rate profile skewed toward earlier crank angles. The numerical constants are a result of using $\Delta\theta_{10-90}$ in the denominator instead of the total combustion duration.

The heat transfer model in the 0D closed-cycle simulation assumes a heat transfer coefficient ($h_{c,i}$) correlation and cylinder gas velocity (w_i) equation proposed by Woschni and provided in [Equation A17](#) and [A18](#), respectively. The mean piston speed (v_p , [Equation A19](#)) was evaluated using the stroke of one piston (v_{1p}) and the engine speed (N) for all three engine architectures. The motoring pressure ($p_{mot,i}$) was calculated directly in the 0D simulation tool using the same method used to calculate the fired cylinder pressure by assuming zero energy release. The heat release rate is calculated for the intake piston (cylinder head for 4S engine), exhaust piston, and liner surfaces using [Equation A20](#). The same heat transfer coefficient is assumed for each surface, although the user-specified metal temperature ($T_{m,n}$) can vary for each surface. The area versus crank angle relationship for each surface ($A_{n,i}$, [Equation A21](#)) are determined using the engine geometries described above.

While it is understood that the Woschni equations were developed for a four-stroke engine with a cylinder head and therefore may not be completely relevant to opposed-piston engines, a comparable heat transfer correlation has not yet been developed for opposed-piston engines and therefore none could be used. Because the same heat transfer correlation was applied to all engine configurations considered, the assumption was considered valid for the thermodynamic comparison contained herein.

Pressure Prediction

$$\left. \frac{dp}{d\theta} \right|_i = \left(\left. \frac{dQ_c}{d\theta} \right|_i - \left. \frac{dQ_{HT}}{d\theta} \right|_i - \frac{\gamma_i}{\gamma_i - 1} p_i \left. \frac{dV}{d\theta} \right|_i \right) \frac{\gamma_i - 1}{V_i} \quad (A1)$$

Table A1. Specific heat capacity curve fit coefficients for the five species of interest, as published by NASA Glenn [16].

		N ₂	O ₂	Ar	CO ₂	H ₂ O
a1	200 K ≤ T < 1000 K	2.210371497E+04	-3.425563420E+04	0.000000000E+00	4.943650540E+04	-3.947960830E+04
	1000 K ≤ T < 6000 K	5.877124060E+05	-1.037939022E+06	2.010538475E+01	1.176962419E+05	1.034972096E+06
a2	200 K ≤ T < 1000 K	-3.818461820E+02	4.847000970E+02	0.000000000E+00	-6.264116010E+02	5.755731020E+02
	1000 K ≤ T < 6000 K	-2.239249073E+03	2.344830282E+03	-5.992661070E-02	-1.788791477E+03	-2.412698562E+03
a3	200 K ≤ T < 1000 K	6.082738360E+00	1.119010961E+00	2.500000000E+00	5.301725240E+00	9.317826530E-01
	1000 K ≤ T < 6000 K	6.066949220E+00	1.819732036E+00	2.500069401E+00	8.291523190E+00	4.646110780E+00
a4	200 K ≤ T < 1000 K	-8.530914410E-03	4.293889240E-03	0.000000000E+00	2.503813816E-03	7.222712860E-03
	1000 K ≤ T < 6000 K	-6.139685500E-04	1.267847582E-03	-3.992141160E-08	-9.223156780E-05	2.291998307E-03
a5	200 K ≤ T < 1000 K	1.384646189E-05	-6.836300520E-07	0.000000000E+00	-2.127308728E-07	-7.342557370E-06
	1000 K ≤ T < 6000 K	1.491806679E-07	-2.188067988E-07	1.205272140E-11	4.863676880E-09	-6.836830480E-07
a6	200 K ≤ T < 1000 K	-9.625793620E-09	-2.023372700E-09	0.000000000E+00	-7.689988780E-10	4.955043490E-09
	1000 K ≤ T < 6000 K	-1.923105485E-11	2.053719572E-11	-1.819015576E-15	-1.891053312E-12	9.426468930E-11
a7	200 K ≤ T < 1000 K	2.519705809E-12	1.039040018E-12	0.000000000E+00	2.849677801E-13	-1.336933246E-12
	1000 K ≤ T < 6000 K	1.061954386E-15	-8.193467050E-16	1.078576636E-19	6.330036590E-16	-4.822380530E-15

$$\left. \frac{dm}{d\theta} \right|_i = \begin{cases} 0, & \theta_i < \theta_{SOI} \\ \frac{m_f}{\Delta\theta_{inj}}, & \theta_{SOI} \leq \theta_i < (\theta_{SOI} + \Delta\theta_{inj}) \\ 0, & \theta_i \geq (\theta_{SOI} + \Delta\theta_{inj}) \end{cases} \quad (A2)$$

$$V_i = f(\theta_i) \quad (A3)$$

$$\left. \frac{dV}{d\theta} \right|_i = \frac{V_{i+1} - V_{i-1}}{\theta_{i+1} - \theta_{i-1}} \quad (A4)$$

$$T_i = \frac{p_i V_i}{m_i R_i} \quad (A5)$$

$$R_i = \frac{\bar{R}}{MW_i} \quad (A6)$$

$$p_{i+1} = p_i + \left. \frac{dp}{d\theta} \right|_i (\theta_{i+1} - \theta_i) \quad (A7)$$

$$m_{i+1} = m_i + \left. \frac{dm}{d\theta} \right|_i (\theta_{i+1} - \theta_i) \quad (A8)$$

$$x_{n,i} = x_{n,0}(1 - x_{b,i}) + x_{n,b}(x_{b,i}) \quad (A9)$$

$$MW_i = \sum_{j=1}^n x_{j,i} MW_{j,i} \quad (A10)$$

$$c_{p,i} = \sum_{j=1}^n y_{j,i} c_{p,j,i} \quad (A11)$$

$$y_{n,i} = x_{n,i} \frac{MW_{n,i}}{MW_i} \quad (A12)$$

$$c_{p,n,i} = R_n \sum_{j=1}^7 a_{j,n} T_i^{j-3} \quad (A13)$$

$$\gamma_i = \frac{c_{p,i}}{c_{p,i} - R_i} \quad (A14)$$

Fluid Properties

Energy Release Rate (Combustion)

$$x_{b,i} = 1 - \exp \left\{ - \left[\left(2.302^{\frac{1}{m_c+1}} - 0.105^{\frac{1}{m_c+1}} \right) \left(\frac{\theta_i - \theta_{SOC}}{\Delta\theta_{10-90}} \right) \right]^{m_c+1} \right\} \quad (A15)$$

$$\left. \frac{dQ_C}{d\theta} \right|_i = \frac{x_{b,i+1} - x_{b,i-1}}{\theta_{i+1} - \theta_{i-1}} (m_f LHV_f) \quad (A16)$$

Heat Transfer Rate

$$h_{c,i} = 5b^{m_{ht}-1} p_i^{m_{ht}} w_i^{m_{ht}} T_i^{0.75-1.62m_{ht}} \quad (A17)$$

$$w_i = 2.28v_p + (3.25 \times 10^{-3}) \frac{V_d T_0}{p_0 V_{tr}} (p_i - p_{mot,i}) \quad (A18)$$

$$v_p = 2v_{1p} N \quad (A19)$$

$$\left. \frac{dQ_{HT}}{d\theta} \right|_i = h_{c,i} [A_{IP,i} (T_i - T_{m,IP}) + A_{EP,i} (T_i - T_{m,EP}) + A_{L,i} (T_i - T_{m,L})] \quad (A20)$$

$$A_{n,i} = f(\theta_i) \quad (A21)$$

The Engineering Meetings Board has approved this paper for publication. It has successfully completed SAE's peer review process under the supervision of the session organizer. This process requires a minimum of three (3) reviews by industry experts.

All rights reserved. No part of this publication may be reproduced, stored in a retrieval system, or transmitted, in any form or by any means, electronic, mechanical, photocopying, recording, or otherwise, without the prior written permission of SAE.

ISSN 0148-7191

Positions and opinions advanced in this paper are those of the author(s) and not necessarily those of SAE. The author is solely responsible for the content of the paper.

SAE Customer Service:
Tel: 877-606-7323 (inside USA and Canada)
Tel: 724-776-4970 (outside USA)
Fax: 724-776-0790
Email: CustomerService@sae.org
SAE Web Address: <http://www.sae.org>
Printed in USA